JOURNAL OF Materials CHEMISTRY

Sodium borohydride reduction of aqueous iron–zirconium solutions: chemical routes to amorphous and nanocrystalline Fe–Zr–B alloys

Glyn D. Forster,[a] Luis Fernández Barquín,[b] Robert L. Bilsborrow,[c] Quentin A. Pankhurst,[a] Ivan P. Parkin*[d] and W. Andrew Steer[a]

[a]*Department of Physics and Astronomy, University College London, Gower Street, London, UK WC1E 6BT*
[b]*Departamento CITIMAC, Facultad Ciencias, Universidad de Cantabria, Santander 39005, Spain*
[c]*CLRC Daresbury Laboratory, Warrington, Cheshire, UK WA4 4AD*
[d]*Department of Chemistry, University College London, 20 Gordon Street, London, UK WC1H 0AJ*

Received 13th May 1999, Accepted 30th June 1999

Fine particle Fe–Zr–B alloys have been prepared by sodium borohydride reduction of aqueous solutions of iron(II) and zirconium(IV) sulfate. A comprehensive survey of reaction conditions was completed and optimum parameters found for the preparation of precipitated products. These included rapid stirring, controlled pH in the range 5–6, using degassed solvents, Fe : Zr ratios between 4 : 1 and 20 : 1 and sodium borohydride concentrations between 0.1 and 1.2 M. Scanning electron microscopy showed that the products comprised spherical particles of 0.1 μm diameter with metal compositions, determined by atomic absorption, electron microprobe and EDAX, which mirrored the initial starting solutions. The products fell into two categories: amorphous Fe–Zr–B alloys when the Fe : Zr ratio was near 9 : 1, and nanocrystalline alloys, comprising a small amount of nanometre scale α-Fe crystallites embedded in amorphous Fe–Zr–B alloy, when the Fe : Zr ratio was either higher or lower than 9 : 1. Minor impurities in the form of Fe(II) complex and Fe(III) oxide phases were also detected in the products. Full structural and magnetic characterisations were performed on selected samples, including X-ray diffraction, Mössbauer spectroscopy, differential scanning calorimetry, magnetometry and Zr-edge EXAFS measurements.

Introduction

Amorphous Fe–Zr–B alloys have attracted great interest due to their inhomogeneous spin structure, which gives rise to low temperature re-entrant spin glass states, and various striking structural and magnetic properties, including broad hyperfine field distributions and high temperature resistivity minima.[1–3] On controlled thermal treatment, these amorphous alloys may be structurally modified to the 'nanocrystalline' state, where nanometre sized crystallites of α-Fe are embedded in the remanent amorphous matrix. In this form the alloys exhibit outstanding soft magnetic properties, with high permeabilities and large saturation magnetisations, which offer clear opportunities in the manufacture of new and improved devices. As such, these nanocrystalline alloys have been the subject of extensive study regarding their production and technological application. Work has focused on the interplay between the different magnetic species in a multiphase alloy, where diverse structural environments including nanocrystalline, amorphous and grain boundaries may all coexist.[1,4,5]

Several production routes have been employed to produce amorphous metallic alloys that constitute the 'precursors' of the metallic nanocrystalline alloys. The most common of these rely on rapid solidification from the liquid or gas phase.[6,7] One such route is 'melt quenching' where a molten sample is rapidly cooled (at around 10^6 K s^{-1}), by dropping the melt onto a rotating metal disc, producing ribbon shaped alloys. Other common routes are sputtering and vapour deposition, where cooling rates of up to 10^8 K s^{-1} are possible, producing thin-film products. Alternative solid state routes have also been explored, such as mechanical alloying, which has been used to produce powder amorphous alloys.[8]

A completely different preparative route to amorphous metallic alloys has recently been developed. This new method involves the formation of fine metal and metal boride particles *via* sodium borohydride reduction in aqueous solution.[9–12] This route holds the additional novelty of producing material in the form of fine powders that may have distinct processing advantages over conventional bulk alloys for the manufacture of net shape devices. The fine particle form also opens a wealth of new possibilities intrinsic to nanoscale magnetism, including applications as ferrofluids, catalysts and recording media,[13,14] as well as fundamental phenomena such as superparamagnetism and spin tunnelling.[15] There is also the potential for the production of amorphous alloys of compositions that are otherwise inaccessible, as shown for the case of high boron content Fe–Co–B and Fe–Ni–B alloys.[11,16] Another feature of the chemical reduction route is that varying the synthesis conditions allows the production of alloys with different structural arrangements, including pure amorphous, multiphase, nanocrystalline and crystalline phases. This possibility is of special interest for the Fe–Zr–B alloys, given their scientific and technological relevance in both the amorphous and nanocrystalline states.

Sodium borohydride is thermodynamically unstable in aqueous solution. However, provided the solution is maintained above pH 5, a short kinetic stability window is available for reduction chemistry. It has been shown that dropwise addition of sodium borohydride to rapidly stirred aqueous solutions of Fe(II) or Fe(III) salts produces a black precipitate of predominantly (*ca.* 80%+) fine particulate amorphous Fe–B.[17] The reaction is rapid and the product is easily isolated by filtration. These reactions give rise to a different set of compositions to those available by other methods. The freshly formed particles are prone to oxidation and are often contaminated with other species that are present in solution.

Indeed, many of the assignments in the literature indicate that the products from borohydride reduction are predominantly multi-component systems of which the amorphous fragment is, under the correct conditions, the predominant phase. Vigorous washing, and in some cases controlled passivation procedures, have been adopted to stabilise the particles. These procedures invariably involve surface oxidation of the particles and hence lead to oxide contamination.

One of the advantages of the chemical reduction route is the facile formation of ternary metal-boride fine particles simply by using a mixture of aqueous metal salts. Systems made to date include Fe–Co–B,[11] Fe–Ni–B,[16] Fe–Cr–B[18], Fe–Mn–B[19] and Fe–W–B,[20] all of which have dominant fine particle amorphous phases. Variation in the metal to metal ratios in these fine particles is possible within a relatively narrow range. We note that the formation of amorphous Fe–Zr–B alloys, which is the subject of this study, may be regarded at the outset as a more difficult task than the formation of ternary alloys with purely first row transition metal elements.

Characterisation of the fine particles prepared by chemical reduction has various levels of complexity as the materials of interest are often multiphase and in some instances can be best described as amorphous metal oxide–borides,[20] or a combination of amorphous plus nanocrystalline phases. Three main methods of analysis have been used to establish the structure of these materials: Mössbauer spectroscopy, X-ray powder diffraction and thermal analysis. The combination of two microscopic techniques with the thermal analyses provides valuable information specifically required for the analysis of multiphase materials. ^{57}Fe Mössbauer spectroscopy exhibits a characteristic amorphous sextet signature and is a powerful technique when dealing with combinations of different Fe-based species. X-Ray powder diffraction shows broad diffraction peaks in the pure amorphous case and also provides information about the size of crystals, even in an amorphous plus nanocrystalline arrangement. Thermal analysis can show a crystallisation exotherm which is characteristic of an amorphous-to-crystalline or amorphous-to-nanocrystalline transformation.

In some instances, for example the materials classified as Fe–W–B alloys,[20] the state of the particles is not entirely clear, although it is certain that the elements are not homogeneously distributed through the product, and that the data could perhaps best be described as indicative of mixed metal oxides. In other materials, such as Fe–Co–B alloys,[11] an extensive series of microscopy, element microprobe mapping, bulk analysis and magnetism studies have pinned down the material as being predominantly (*ca.* 95%) amorphous.

In this paper we report our studies on the formation of a new class of Fe–Zr–B fine particles by the sodium borohydride reduction of aqueous solutions of iron and zirconium sulfates. Our primary motivation has been to develop a series of materials with compositions potentially different from those obtained from conventional routes, and which could be prepared as either amorphous or nanocrystalline structures. Typically, conventional routes such as melt spinning produce materials with low boron contents, up to 10 at.% boron. Our interest is based both on the scientific merit of the system, given the extremely varied magnetic states known for the Fe–Zr and Fe–Zr–B alloys,[3] and on the technological potential of nanocrystalline Fe–Zr–B alloys in soft magnetic applications. The work builds on our earlier study of the formation of amorphous Fe–Zr–B by chemical reduction,[21] with the added dimension of exploring the nanocrystalline materials, as well as providing a much more detailed investigation of the variations in the reaction chemistry. Our goal here is to understand and speculate on the reaction mechanism. To this end, and in contrast to other researchers in this area, we have conducted chemical reduction syntheses using fully anaerobic Schlenk line procedures. We have also maintained careful monitoring of the reaction pH, and have endeavoured to fully analyse all of the phases produced in the reactions.

Experimental

Reagents were purchased from Aldrich Chemical Co., and used as supplied. Water was distilled and purged with argon for 3 h prior to use. Anaerobic preparations were carried out using standard Schlenk line techniques under an argon atmosphere. Manipulation of samples was performed in a Saffron glove box under an argon atmosphere.

Scanning electron microscopy was carried out on a Hitachi S-4000. Electron microprobe analysis was carried out on a JEOL EMA by taking a series of 500 measurements using a 1 μm^2 beam passing across the surface of a pressed sample. Atomic absorption analysis was performed on a PYE Unicam SP9 Atomic Absorption Spectrophotometer using samples prepared by dissolving *ca.* 30 mg of material in 5 ml of 37% HCl, subsequently diluted up to 10 ml. Standards were prepared from iron(II) sulfate heptahydrate, zirconyl chloride octahydrate and boric acid and prepared as the samples. FT-IR spectroscopy was performed on a Nicolet 205 FT-IR using pressed potassium bromide pellets.

Room temperature ^{57}Fe Mössbauer spectra were collected on a Wissel MR-260S constant acceleration spectrometer, calibrated against α-iron, with the sample contained in an argon-filled stainless steel container with Mylar windows. A triangular drive waveform was used and the spectra were folded to remove baseline curvature. The spectra were analysed using a least-squares fitting program based on combination of Lorentzian sextets and doublets for the subspectra of magnetically ordered crystalline or paramagnetic phases, respectively, plus a broad Voigtian sextet for the amorphous phase. The Voigtian profiles were constrained to assume physically realistic line positions and linewidths, in keeping with a standard model for amorphous metallic materials.[22]

X-Ray diffraction patterns were recorded on a Philips X-pert θ–θ reflection diffractometer with Mo-Kα radiation ($\lambda = 0.7107$ Å) using an argon-filled sample chamber. Further X-ray studies on the creation of nanocrystalline Fe–Zr–B alloys were performed on Station 9.1 at the Daresbury Laboratory, UK, using synchrotron radiation tuned to $\lambda = 0.4868$ Å. Selected samples were sealed under argon into quartz capillary tubes, then heated in a tube furnace to 400 or 500 °C at a rate of 10 K min^{-1}. These samples were then removed from the furnace and allowed to rapidly cool to room temperature. The samples, still in their capillaries, were exposed on a new image-plate Debye–Scherrer powder diffraction camera on Station 9.1, which provided an excellent signal to noise ratio with rapid throughput (typically 15 min) and a wide dynamic range.[23] This enabled the preliminary identification of some of the minority constituent crystallisation products in the samples.

Differential scanning calorimetry was performed on a Shimadzu DSC-50 from 20 °C to 600 °C at a heating rate of 10 K min^{-1}, with the sample kept under argon in a sealed stainless steel crucible with gold seals. The samples, which were loaded under argon in a glove box, were typically of the order of 10–20 mg in mass. Some difficulties were encountered in accurately measuring these masses anaerobically inside a glove box, so that the data presented here should be regarded as qualitative rather than quantitative.

Hysteresis measurements were made at room temperature in fields up to 5 kOe using an Aerosonic 3001 vibrating sample magnetometer. Magnetisation data were recorded in an external field of 100 Oe using a Quantum Design MPMS SQUID magnetometer with zero field cooled (ZFC) and field cooled (FC) sequences. For the FC runs, 100 Oe was applied at 300 K and the sample cooled to 10 K, then measurements were recorded, with the 100 Oe field still applied, on heating back to

300 K. For the ZFC runs the sample was cooled to 10 K in zero field, then 100 Oe was applied and the data recorded as the temperature rose to 300 K.

Some preliminary room temperature zirconium K-edge EXAFS data were collected on Station 16.3 at the Daresbury Laboratory, UK, using the transmission mode. The data were analysed using the Daresbury EXCALIB[24] and EXBACK[25] software packages to obtain the Fourier transformed radial structure functions about the Zr atoms.

Aerobic preparation

Details of a representative reaction are as follows. Iron(II) sulfate heptahydrate (10.01 g, 36.0 mmol) and zirconium(IV) sulfate hydrate (1.13 g, 3.64 mmol) were dissolved in water (100 ml). To this rapidly stirred solution was added aqueous sodium hydroxide (*ca.* 2.0 M) until the pH reached 6.0. A solution of sodium borohydride (2.28 g, 60.0 mmol) in water (100 ml) was then added dropwise over a period of 30 min, resulting in the precipitation of a fine black solid. The pH of the solution was monitored during the course of the reaction and kept at around 6.0. After the addition the black solid was collected by filtration and washed with water (5×200 ml) and acetone (100 ml). The yield of product was 3.40 g. The solid was stored in a glove box to limit further oxidation.

Anaerobic preparations

Details of a representative reaction are as follows. A 500 ml three neck round bottom flask equipped with a pressure equalised dropping funnel, a gas tubing adapter and a pH meter probe, was charged with iron(II) sulfate heptahydrate (10.01 g, 36.0 mmol), zirconium(IV) sulfate hydrate (1.13 g, 3.64 mmol) and degassed water (100 ml). The pH of this rapidly stirred solution was adjusted to 6.0 *via* the addition of a degassed solution of sodium hydroxide (*ca.* 2.0 M). The dropping funnel was charged with sodium borohydride (2.28 g, 60.0 mmol) in degassed water (100 ml), which was added dropwise to the solution over a period of 30 min, causing the precipitation of a black solid. After the addition was complete the black solid was collected by filtration and washed with water (5×200 ml) and acetone (100 ml), yielding 3.52 g of product. The solid was stored in a glove box to limit further oxidation.

A series of experiments was conducted using the procedure outlined above but at different pH, stirring rates, volume of solution and initial molar concentrations of the reagents. The pH of the initial solution was also controlled by addition of the sodium borohydride solution (pH 12) rather than sodium hydroxide.

CAUTION Fine metallic particles can be pyrophoric. Both the aerobically and anaerobically prepared Fe_xZr_yB particles were in some cases found to undergo spontaneous self annealing and generate temperatures in excess of 600 °C. This self annealing was often triggered by exposure to air. The material can be partially passivated, if required, by passing argon (0.01% O_2) over the material for 24 h.

Results

Dropwise addition of an aqueous solution of sodium borohydride to a stirred solution of iron and zirconium sulfates produced a black precipitate. The experiments were conducted at various different pH, reagent concentrations, air sensitive handling conditions and stirring rates. The precipitates were collected by filtration and analysed by a wide range of techniques, including SEM/EDAX, atomic absorption, electron microprobe analysis, FT-IR, ^{57}Fe Mössbauer spectroscopy, X-ray diffraction, differential scanning calorimetry, vibrating sample magnetometry, SQUID magnetometry and Zr-edge EXAFS.

Fine particles prepared under rigorous anaerobic conditions had different compositions and properties compared to aerobically prepared materials, the most notable being their behaviour under oxidation. The anaerobic particles underwent vigorous oxidation, sometimes glowing red or catching fire, on exposure to air, whilst the aerobically prepared particles seemed relatively air stable.

Survey of reaction conditions

The reaction of sodium borohydride with aqueous solutions of $FeSO_4$ and $Zr(SO_4)_2$ was achieved in one of two ways. The pH was either controlled, using sodium hydroxide or hydrochloric acid, or the pH was allowed to vary in response to the addition of the reactant sodium borohydride solution, which has an intrinsic pH of 12.

At initial pH values controlled to be greater than 6.0, a mirror-like metallic film was formed on the walls of the reaction vessel and yields of fine metallic particles were low. At pH values controlled to be lower than 4.0 the products from the reaction were fine black powders which contained many components including Fe(II) and Fe(III) phases (*ca.* 30% by Mössbauer spectroscopy). In reactions in which the pH was not controlled, it was found to remain fairly constant between 5.5 and 6.2 throughout the addition of sodium borohydride. It should be noted that some variation of pH would be expected in the solution and that these local variations may be the cause of some of the multiphase products. It was found that vigorous stirring using an overhead paddle stirrer or a magnetic follower ensured a more homogeneous product. Care was taken not to add an excess of sodium hydroxide to aqueous solutions of $FeSO_4$ and $Zr(SO_4)_2$ as it produces a white precipitate (pH>8) that contains both iron and zirconium oxides.

Under standard conditions, with the pH controlled at 6.0, noticeable reaction occurred on addition of the first few drops of the sodium borohydride solution to the rapidly stirred mixed metal sulfate solution. This produced a fine black precipitate throughout the whole solution. After the addition of 4–5 drops of sodium borohydride solution (1.0 M) the initial pale green colour of the starting solution was masked by the precipitate. Further addition of sodium borohydride produced more precipitate. Noticeably the precipitate was free flowing, non-agglomerated and did not flocculate. On standing the precipitate did settle but the solution maintained a darkened coloration, possibly due to nanoparticulates.

In addition to the experiments described above, a series of Fe–Zr–B alloys were made without controlling the initial pH of the solution. Fig. 1 shows a plot of the pH against amount of added sodium borohydride. This figure shows that the initial mixed iron/zirconium sulfate solution is acidic (pH 2.5). Addition of aqueous sodium borohydride (pH 12) increases the pH of the iron–zirconium solution until a pH of between 5.5 and 6.0 is obtained. At this point, as the pH just fails to rise

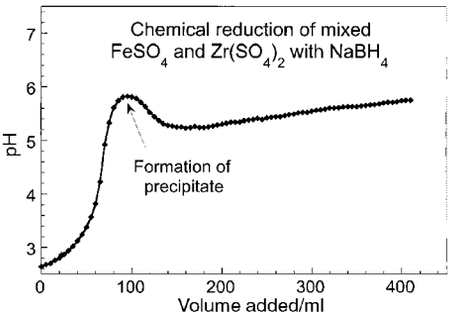

Fig. 1 Chemical synthesis of Fe–Zr–B, illustrated as a plot of solution pH against amount of added sodium borohydride, for the reduction of 36 mmol of iron(II) sulfate and 4 mmol of zirconium sulfate in 100 ml of water.

with addition of sodium borohydride, precipitation of the black amorphous alloy starts. The precipitate was identical to that of the reactions where the initial pH was raised to 6.0. Precipitation continues as more sodium borohydride is added and the pH of the solution actually falls, despite addition of a basic solution. The pH of the solution then remains relatively unaltered with addition of successive amounts of sodium borohydride ending up with a final pH of 5.5–6.0.

It was possible to vary the starting Fe : Zr molar ratio of the reagents and still get a fine black particulate product. Ratios of Fe : Zr from 4 : 1 to 20 : 1 were investigated. It was found that higher zirconium content solutions had lower initial pH values. This was a function in part of a small amount of residual sulfuric acid in the commercial zirconium sulfate. Fe : Zr ratios below 4 : 1 produced inhomogeneous white/black precipitates. Changes in the molarity of the initial sodium borohydride solution from 0.1 to 1.2 M were investigated. These studies showed that the reaction was largely independent of sodium borohydride concentration provided that the sulfate solutions were well stirred. At higher concentrations and for less well-stirred solutions a more multiphase product was seen.

The most viable conditions for the preparation of fine particulate samples was to ensure rapid stirring; degassed solvents, an Fe : Zr ratio between 4 : 1 and 20 : 1, and a sodium borohydride concentration of between 0.1 and 1.2 M. Samples could be prepared using either Schlenk line techniques or by doing the reaction in air but employing degassed solvents. The samples prepared using Schlenk conditions were prone to violent oxidation.

Aqueous sodium borohydride solution has a pH of 12. It slowly evolves hydrogen and forms the basic metaborate anion. Addition of this solution to aqueous mixed iron–zirconium sulfate solutions evolves large quantities of hydrogen. This may be a consequence of two factors. Firstly the acidic pH of the sulfate solutions encourages decomposition of the sodium borohydride forming hydrogen. Secondly the sodium borohydride solution also acts as a reducing agent to form the fine metal particles.

Yields of the fine black powders were 30–40%. The powders were isolated by Buchner filtration followed by drying in the antechamber of a glove box. The black powders underwent oxidation in air after evaporation of residual amounts of water. In that case some of the material became orange in colour. The filtrate from the reaction was initially a pale orange in colour. This became a darker orange on standing in air and precipitated an orange solid that was identified as a mixture of iron oxides and hydroxides [$Fe(OH)_3$]. Evaporation of the filtrate yielded some iron and zirconium sulfate, iron oxide and white crystals of sodium sulfate. The limiting reagent in the reaction was the sodium borohydride.

The compositions of the fine particle products were determined by a combination of electron microprobe, EDAX and atomic absorption measurements. The amounts of boron incorporated in the products were of the order of 25–30 at.%. The Fe : Zr composition of the fine powders mimicked the initial molar concentrations of the starting solutions save for a slight enhancement in Fe (*e.g.* observed Fe : Zr 9.13 : 1, expected 9 : 1). Notably, under optimum conditions, negligible amounts of sulfur were detected in the product (less than 0.5%). However, if the pH range was outside the 4–6 window, or if the precipitate was not washed thoroughly, up to 5% sulfur was detected in the product, probably coming from coprecipitated metal sulfide.

Characterisation of amorphous and nanocrystalline fine particles

For the remainder of the paper we concentrate on four representative Fe–Zr–B samples prepared by the chemical reduction of aqueous iron–zirconium solutions. Two of these are selected as typical examples of products which are predominantly amorphous fine particles, while the other two are selected as examples of nanocrystalline fine particles. The compositions of these samples, as measured by electron microprobe, EDAX and atomic absorption, were $Fe_{59}Zr_6B_{35}$, $Fe_{63}Zr_7B_{30}$, $Fe_{54}Zr_{11}B_{35}$ and $Fe_{62}Zr_3B_{35}$. Details of the preparation conditions used are given in Table 1.

Scanning electron micrographs showed that the products were made up of 3 μm agglomerates of roughly spherical particles of dimension 0.1 μm. FT-IR analysis showed no absorptions due to water or sulfate, and exhibited only broad bands at 700–600 cm^{-1}, which could be attributed to metal boron vibrations.

Electron microprobe line analysis using a 1 μm beam spot scanned over 500 or more points was used to provide information on the homogeneity of the samples. Measurements were made using the Fe K_α and Zr L_α emission lines, for which the observed count rate varied linearly with elemental percentage. These emission lines were chosen to allow simultaneous detection of both elements from the same beam

Table 1 Preparation conditions, composition determined by EDAX and atomic absorption, and Mössbauer effect and magnetometry parameters for the products of sodium borohydride reduction of aqueous iron and zirconium sulfates. The Mössbauer parameters are the area percentage of the amorphous phase in the room temperature spectrum, the mean hyperfine field B_{hf}, the rms deviation in the hyperfine field ΔB_{hf} and the isomer shift δ for that phase. The magnetometry parameters are the maximum magnetisation σ_{max} and the coercivity H_c determined from a hysteresis loop recorded in a field of up to ± 5 kOe

Preparation conditions and deduced compositions				
Aerobic/Anaerobic	Aerobic	Anaerobic	Anaerobic	Anaerobic
Moles of $FeSO_4$	36.0	35.9	35.9	35.9
Moles of $Zr(SO_4)_2$	4.00	4.01	7.97	1.99
Moles of $NaBH_4$	60.0	60.3	60.5	58.3
Initial Fe/Zr ratio	9	9	4.5	18
Initial Fe/B ratio	0.60	0.60	0.59	0.62
Fe/Zr ratio (EDX)	9.4	9.13	4.92	18
Fe/B ratio (AA)	1.69	2.15	1.54	1.74
Deduced composition	$Fe_{59}Zr_6B_{35}$	$Fe_{63}Zr_7B_{30}$	$Fe_{54}Zr_{11}B_{35}$	$Fe_{62}Zr_3B_{35}$
Mössbauer spectroscopy results				
% Amorphous phase	89(1)	86(1)	73(2)	81(1)
B_{hf}/kG	208(1)	235(1)	222(1)	222(1)
ΔB_{hf}/kG	100(2)	89(2)	95(7)	103(2)
δ/mm s^{-1}	0.16(1)	0.09(1)	0.13(1)	0.11(1)
Magnetisation results				
σ_{max}/emu g^{-1}	74(2)	132(3)	—	127(3)
H_c/Oe	170(5)	190(5)	—	285(5)

spot, thus eliminating any errors due to movement of the sample stage between measurements. The information obtained from the Fe and Zr linescans are presented in the form of scatter plots in Fig. 2. In all cases relatively tight elemental distributions are seen, with no evidence of phase segregation as would be evidenced by points with zero contribution from either the Fe or Zr lines. The elemental distributions observed for $Fe_{59}Zr_6B_{35}$ and $Fe_{63}Zr_7B_{30}$ are especially tight, and are of the same order as those observed for materials regarded as archetypal amorphous alloys by chemical reduction, such as Fe–Ni–B.[21]

Room temperature ^{57}Fe Mössbauer spectra of the Fe–Zr–B samples are shown in Fig. 3. The spectra of $Fe_{59}Zr_6B_{35}$ and $Fe_{63}Zr_7B_{30}$ are almost entirely composed of a broadened magnetic sextet, which is typical of an amorphous alloy. The spectra of the other samples, $Fe_{54}Zr_{11}B_{35}$ and $Fe_{62}Zr_3B_{35}$, differ mainly in the presence of an additional sextet pattern with outermost lines at ± 5.3 mm s^{-1}, which is an unambiguous sign of α-Fe. The presence of this α-Fe component is particularly interesting as a possible indicator of nanocrystallisation. It is clear that the α-Fe must be homogeneously spread throughout the particles, and at least sub-micron sized, to account for the electron microprobe data showing no signs of phase segregation on the micron scale. It is a particular feature of Mössbauer spectroscopy that even nanometre scale crystalline phases may be unambiguously distinguished in these systems.

Smaller contributions appear in all four spectra due to an iron(II) phase doublet, and an iron(III) oxide doublet. The Mössbauer parameters for the iron(II) doublets are: isomer shift $\delta = 1.10 \pm 0.02$ mm s^{-1}, quadrupole splitting $\Delta = 2.48 \pm 0.14$ mm s^{-1}. These values do not match with literature figures for either iron(II) sulfate $FeSO_4$ ($\delta = 1.27$ mm s^{-1}, $\Delta = 2.73$ mm s^{-1}) or iron(II) sulfate heptahydrate $[Fe(H_2O)_6]$-$SO_4 \cdot H_2O$ ($\delta = 1.26$ mm s^{-1}, $\Delta = 3.22$ mm s^{-1}).[26] In part to cast more light on the identity of this phase, oxidation experiments were performed on both the aerobic $Fe_{59}Zr_6B_{35}$ and anaerobic $Fe_{63}Zr_7B_{30}$ samples.[21] On exposure to air, the aerobic sample showed no sign of reaction, and required several days before differences could be measured in its Mössbauer spectrum. However, after exposure to air for 30 days, the iron(II) phase had decreased in spectral area while the area of the iron(III) phase had increased by a comparable amount. Such oxidation behaviour is not expected for iron(II) sulfate, and we surmise

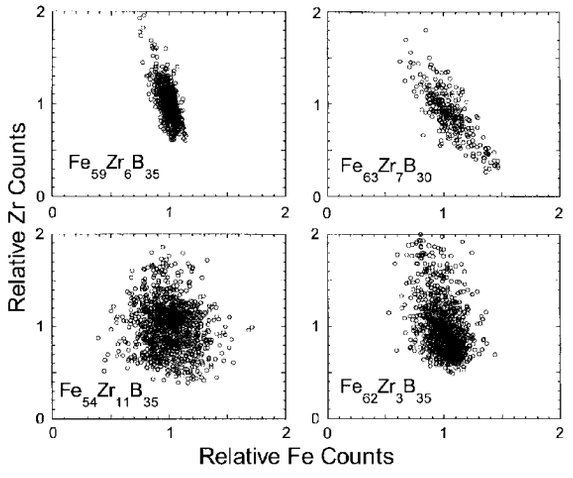

Fig. 2 Electron microprobe homogeneity data on the micron scale spatial distribution of Fe and Zr atoms in Fe–Zr–B fine particle samples prepared by chemical reduction. In none of the scans is there any sign of micron scale phase segregation, as would be evidenced by points with relative Fe or Zr counts at the 0.1 to 0.2 level. It is notable that the amorphous alloys, $Fe_{59}Zr_6B_{35}$ and $Fe_{63}Zr_7B_{30}$, are more homogeneous than the nanocrystalline alloys, $Fe_{54}Zr_{11}B_{35}$ and $Fe_{62}Zr_3B_{35}$.

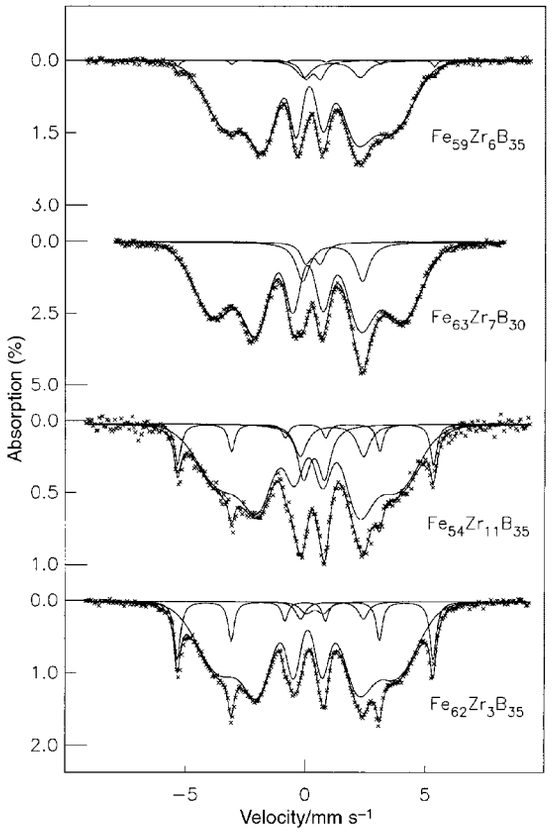

Fig. 3 Room temperature ^{57}Fe Mössbauer spectra of Fe–Zr–B fine particles prepared by chemical reduction. Solid lines are the result of a least-squares fit. The alloys $Fe_{59}Zr_6B_{35}$ and $Fe_{63}Zr_7B_{30}$ are dominated by a broad sextet typical of an amorphous metallic phase. This phase also dominates the $Fe_{54}Zr_{11}B_{35}$ and $Fe_{62}Zr_3B_{35}$ samples, accompanied by a sharp sextet due to α-Fe, as expected in nanocrystalline alloys. Two small impurity phases are also evident, *viz.* doublets due to an Fe(II) complex and an Fe(III) oxide.

that the iron(II) phase is not a sulfate but rather a complex of some form that oxidises over a period of weeks. On exposure to air, the anaerobic sample immediately glowed red. The Mössbauer spectrum recorded on an aliquot exposed to air for 5 minutes showed a large increase in the α-iron phase at the expense of the other phases.

The presence of an iron(III) oxide phase in both the aerobic and the anaerobic Fe–Zr–B samples, the latter having been handled under argon at all times, indicates that the oxide may originate in a side reaction with the water. In $Fe_{59}Zr_6B_{35}$, $Fe_{63}Zr_7B_{30}$ and $Fe_{54}Zr_{11}B_{35}$ the lines of the oxide doublet are relatively sharp, indicating that the phase is crystalline, while in $Fe_{62}Zr_3B_{35}$ the lines are both smaller in area and broad, the latter indicating a disordered environment. One explanation for this could be that the oxides form as dispersed surface contaminants, before forming microcrystallites.

Mo Kα X-ray powder diffraction data for the as-made Fe–Zr–B samples are shown in Fig. 4. Very broad diffraction peaks are seen for $Fe_{59}Zr_6B_{35}$ and $Fe_{63}Zr_7B_{30}$, which are characteristic of amorphous alloys. Similar broad peaks are also apparent in the $Fe_{54}Zr_{11}B_{35}$ and $Fe_{62}Zr_3B_{35}$ data, with the additional presence of some sharper peaks superimposed on the broad peaks. The positions of these peaks coincide with those expected from crystalline α-Fe. The lattice parameters of the α-Fe components have been determined by the $\cos\theta - \text{cotan}\,\theta$ method[27] using the (110), (200) and (211) diffraction peaks. For $Fe_{54}Zr_{11}B_{35}$ $a = 2.870(5)$ Å and for $Fe_{62}Zr_3B_{35}$ $a = 2.904(5)$ Å. These compare very favourably with literature values for bulk α-Fe of $a = 2.866$ Å. Analysis of the (110) peak at 21°, using the

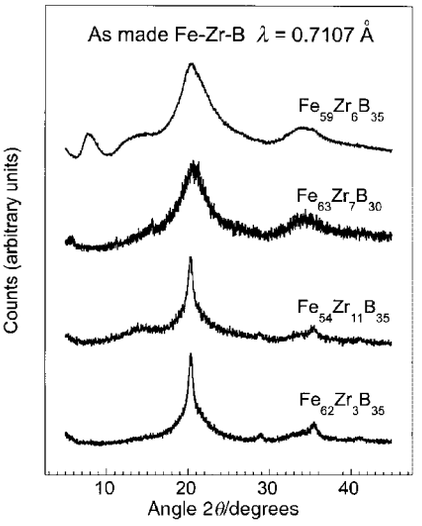

Fig. 4 X-Ray diffraction patterns, recorded using Mo-Kα radiation on a θ–θ reflection diffractometer, of Fe–Zr–B fine particles prepared by chemical reduction. The uppermost two patterns show that the samples are entirely amorphous to the resolution of the diffractometer. The remaining samples show a combination of broad peaks due to an amorphous phase and sharper peaks due to nanocrystalline α-Fe.

Scherrer relation, provides an estimate of the size of the crystallites. Assuming negligible broadening due to lattice strain effects, crystallite sizes of the order of 7 and 6 nm are estimated for $Fe_{54}Zr_{11}B_{35}$ and $Fe_{62}Zr_3B_{35}$, respectively.

Synchrotron X-ray powder diffraction data of as-made and thermally treated aliquots of the $Fe_{54}Zr_{11}B_{35}$ sample are shown in Fig. 5. After treatment at 400 °C the crystalline peaks due to α-Fe grow at the expense of the amorphous phase, and become somewhat sharper, with linewidths that correspond to crystallites of the order of 13 nm in size. After treatment at 500 °C the amorphous phase is negligible, and the diffraction pattern is dominated by peaks due to crystalline α-Fe. Additionally, some minority phase crystallisation peaks are visible in the 2θ range from 14 to 18°. Preliminary scrutiny of these peaks has yielded positive identification of crystalline Fe_3B and ZrO_2, although other iron borides of less defined composition cannot be ruled out in samples with such small grain sizes.

DSC thermograms for the four as-made samples are shown in Fig. 6. A single exothermic peak is seen at 470 °C for the

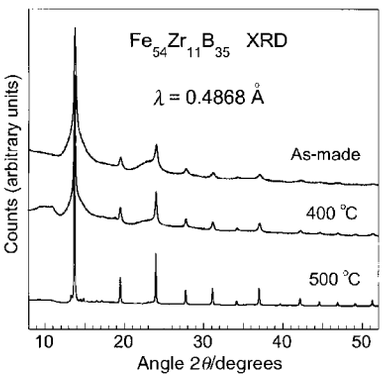

Fig. 5 X-Ray diffraction patterns, recorded using the synchrotron radiation source at Daresbury Laboratory, of nanocrystalline $Fe_{54}Zr_{11}B_{35}$ fine particles, prepared by chemical reduction, in the as-made state and after thermal treatment at 400 and 500 °C. The data show that on heating the nanocrystalline α-Fe phase grows at the expense of the amorphous phase. Some minority phase crystalline peaks due to various Fe–B phases and ZrO_2 are discernible for 2θ between 14 and 18° in the 500 °C sample.

$Fe_{59}Zr_6B_{35}$ sample. Single peaks such as these are characteristic of spontaneous and homogeneous crystallisation in an amorphous alloy, as has been reported in melt-spun Fe–Zr–B alloys.[28,29] In contrast, the $Fe_{62}Zr_3B_{35}$ sample shows two clear peaks, at 470 and 560 °C. Such behaviour is reminiscent of that seen in nanocrystalline alloys, where the first peak relates to the formation of dispersed nanoscale crystallites in the amorphous matrix and the second relates to percolation grain growth and crystallisation throughout the bulk of the material.[2] The DSC data obtained for the other two samples, $Fe_{63}Zr_7B_{30}$ and $Fe_{54}Zr_{11}B_{35}$, are less clear cut, although both show an exotherm in the vicinity of 470 °C and further features at higher temperatures.

Zirconium-edge EXAFS data were obtained for an aerobically prepared Fe–Zr–B sample of a similar composition to the $Fe_{59}Zr_6B_{35}$ sample. For comparison, data were also collected on a sample of crystalline ZrO_2. Radial structure functions are shown in Fig. 7, along with preliminary fits of the data to simple models of the Zr environment. It is clear on inspection that the Zr in the Fe–Zr–B sample exists in a form that is different from that of either Zr metal or ZrO_2. Preliminary analysis indicates that the data are consistent with the Zr atoms being fully incorporated into an amorphous FeZr-based matrix. Further experiments are scheduled to collect more EXAFS data on this system.

Room temperature hysteresis loop measurements on $Fe_{59}Zr_6B_{35}$, $Fe_{63}Zr_7B_{30}$ and $Fe_{62}Zr_3B_{35}$ showed that they were all soft magnets with low coercivities, as given in Table 1. Interestingly, the maximum magnetisation of the amorphous $Fe_{59}Zr_6B_{35}$ sample was only half that of the other two. This is consistent with a predominantly amorphous state, compared to the nanocrystalline state, where high saturation magnetisations are typically seen because of the presence of single domain crystalline α-Fe. Somewhat surprising in this context was the high magnetisation of the $Fe_{63}Zr_7B_{30}$ sample. The implication is that this sample is not as fully amorphous as the $Fe_{59}Zr_6B_{35}$ sample, and that some incipient nanocrystallisation is present. In fact, signs of such a state have already been noted in the Mössbauer data of Fig. 3 and the DSC data of Fig. 6.

SQUID DC-magnetisation measurements were recorded on the amorphous $Fe_{59}Zr_6B_{35}$ and $Fe_{63}Zr_7B_{30}$ samples under zero field cooled (ZFC) and field cooled (FC) conditions, as shown in Fig. 8. The data show substantial divergence between the

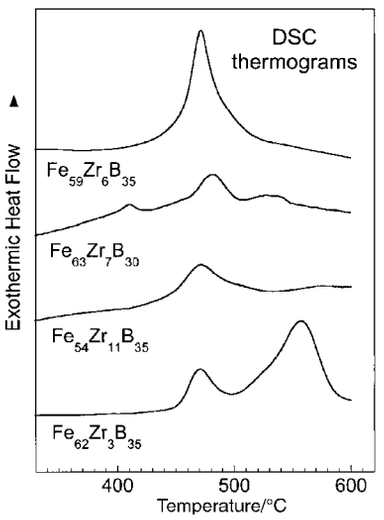

Fig. 6 Differential scanning calorimetry data for Fe–Zr–B fine particles prepared by chemical reduction. The single sharp exotherm near 470 °C for the $Fe_{59}Zr_6B_{35}$ sample is characteristic of crystallisation in a purely amorphous alloy. The two peaks seen for the $Fe_{62}Zr_3B_{35}$ sample are reminiscent of the two-stage crystallisation process encountered in nanocrystalline alloys.

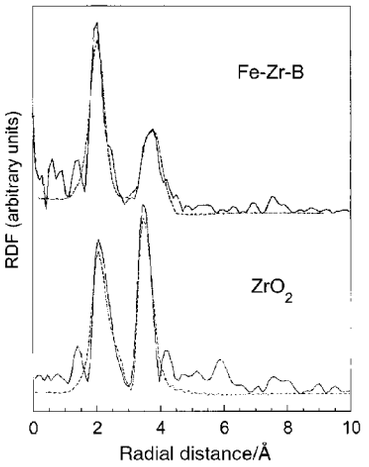

Fig. 7 Room temperature Zr-edge EXAFS data for an amorphous Fe–Zr–B alloy sample, prepared by chemical reduction, compared to polycrystalline ZrO_2. The data show the radial distribution functions around the Zr atoms. The dashed lines correspond to simple models for the Zr environments, which in the case of the Fe–Zr–B alloy assumes that the Zr atoms are fully incorporated into the Fe-based amorphous phase.

ZFC and FC curves, which is a typical feature of superparamagnetic fine particles. The fact that none of the pairs of ZFC/FC curves coincides, even at 300 K, indicates that the blocking temperatures of both samples are above room temperature. In our curves, the blocking temperature is still not observed when increasing the field to 100 Oe, although it is true that the splitting ZFC/FC becomes narrower in such a situation. This can be related to the fact that increasing the applied field tends to lower the blocking temperature in superparamagnetic systems.[15] The knee observed at 30 K in the ZFC curves of $Fe_{59}Zr_6B_{35}$ is reminiscent of signals seen from re-entrant spin glass states in melt-spun Fe–Zr alloys.[30] However, we note that this feature might also be due to a blocking transition in a fraction of the sample that comprises very small particles.

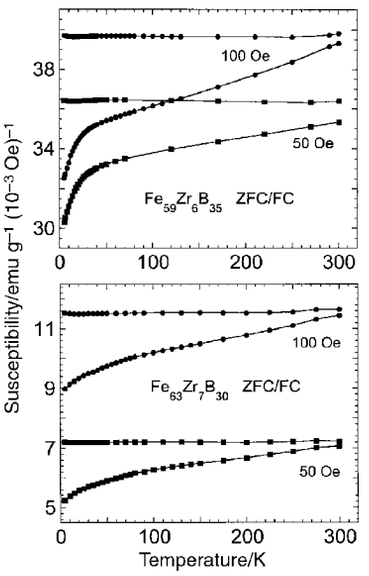

Fig. 8 SQUID magnetisation data for amorphous $Fe_{59}Zr_6B_{35}$ and $Fe_{63}Zr_7B_{30}$ fine particles prepared by chemical reduction. For each sample the data were recorded in applied fields of 50 and 100 Oe. In each case the upper curves as plotted were recorded under field cooled (FC) conditions, and the lower curves were recorded in zero field cooled (ZFC) conditions. The observed splittings between the ZFC and FC curves are typical of fine particle superparamagnetic behaviour.

Discussion

Mechanistic discussion on the sodium borohydride reduction of iron salts in aqueous solutions to produce amorphous or nanocrystalline alloys is underdeveloped. Current thinking indicates that the reaction proceeds *via* iron hydroborate intermediates of the form $[(H_2O)_5Fe(HOBH_3)]^{2+}$. These intermediates have not yet been isolated, primarily because the reaction is extremely rapid. In non-aqueous solutions, such as glyme solvents, discrete borohydride complexes of iron can be isolated, such as $[FeL_n(BH_4)_2]$ where L = solvent ligation. On addition of water to these solutions, amorphous and crystalline iron and iron borides can be isolated.

An overall idealised equation for the reaction is proposed below. This takes into account the isolated [$Fe_{10}ZrB_5$, $Na_2(SO_4)$] and observed (H_2) products from the reaction for a 10 : 1 molar ratio of the initial starting materials. It should be noted that numerous side reactions can also occur in solution. The presence of unwanted oxygen in the solution oxidises the fine metallic particles and forms metal oxides. The reaction does not always go to completion and some residual unreacted Fe(II) components have been detected by Mössbauer spectroscopy.

$$24NaBH_4+10Fe(SO_4)+Zr(SO_4)_2+38H_2O\rightarrow$$
$$Fe_{10}ZrB_5+12Na_2(SO_4)+76.5H_2+19HBO_2$$

The total metal to boron elemental compositions obtained by the chemical reduction of aqueous solutions of iron and zirconium sulfates, M/B = 1.5–1.85, match well the metal/boron ratios obtained in forming Fe–Co–B ($Fe_{44}Co_{19}B_{37}$; M/B = 1.7) and Fe–Ni–B ($Fe_{36}Ni_{28}B_{36}$; M/B = 1.8) when utilising sodium borohydride solutions under similar conditions. This indicates that a common mechanism is probably operating in these reactions. At lower sodium borohydride concentrations, alloys with lower boron contents were obtained.

The synthesised fine particles are predominantly composed of homogeneous Fe–Zr–B alloy, with or without a small fraction of nanometre sized α-Fe crystallites, and some trace impurities of Fe(II) complex and Fe(III) oxides. In equivalent studies of the formation of fine particle Fe–Co–B and Fe–Ni–B amorphous alloys,[11,16] evidence for alloying between the metallic and boron constituents has been based on the presence of the same characteristic signatures in X-ray diffraction, Mössbauer spectroscopy and DSC experiments as seen in this work for Fe–Zr–B. We have gone beyond these standard techniques to consider additional supporting data from EDAX and electron microprobe mapping experiments. The compositional mapping shown in Fig. 2 reveals a relatively homogeneous pattern with virtually complete mixing of Fe and Zr at the 1 μm level. Furthermore, Zr-edge EXAFS data have been recorded and were found to be inconsistent with either metallic Zr or Zr oxide, indicating that the Zr is in a more complex environment. Taken together, the experimental data are therefore indicative of the formation of an amorphous Fe–Zr–B alloy.

One piece of chemical evidence that strongly argues in favour of this is the fact that the variation of the Fe to Zr ratio of the solutions matches the ratio found in the products (Table 1). If the reaction were to occur by the selective reduction of Fe in solution to form, for example, amorphous Fe-B with some incorporated Zr species, it would be unexpectedly fortuitous for the Fe–Zr ratio in the products to mirror the starting solutions. The close correlation therefore implies that there is some form of co-reduction of zirconium and iron in the formation of Fe–Zr–B.

As the result of a comprehensive survey of chemical reduction syntheses of a wide range of Fe–Zr–B alloys, we have noted that the products obtained may be classified into two main categories. The first, exemplified in this paper by the

samples $Fe_{59}Zr_6B_{35}$ and $Fe_{63}Zr_7B_{30}$, are almost entirely amorphous alloys, as revealed by the characteristic broad peaks of the X-ray diffraction spectra and the dominant amorphous sextet in the Mössbauer spectra. The second, exemplified by $Fe_{54}Zr_{11}B_{35}$ and $Fe_{62}Zr_3B_{35}$, may be considered to be directly synthesised nanocrystalline alloys containing a small amount of α-Fe crystallites embedded in the Fe–Zr–B amorphous alloy host. The α-Fe crystallites have sizes below 10 nm, as deduced from X-ray analysis using the Scherrer formula. DSC data confirm the X-ray and Mössbauer findings, with a single exothermic peak signifying an amorphous-to-crystalline transformation for $Fe_{59}Zr_6B_{35}$ and two exothermic peaks in $Fe_{62}Zr_3B_{35}$ being reminiscent of the two stage crystallisation process seen in melt-spun nanocrystalline Fe–Zr–B alloys. The other two samples could be considered as intermediate cases between these.

From our studies we believe that the single most definitive factor determining whether the product of the borohydride reduction of aqueous iron and zirconium sulfates will be an amorphous or a nanocrystalline alloy is the ratio of Fe to Zr atoms in the starting mixture. It is evident from Table 1 that the amorphous alloys are formed when the Fe : Zr ratio is of the order of 9 : 1, whereas using an Fe : Zr ratio either above or below this results in the nanocrystalline state. The relatively large size difference between the Fe and Zr atoms is clearly a factor here, with the implication being that there are well defined upper and lower limits to the compositional range within which an amorphous Fe–Zr–B alloy will exist.

A comparison between the magnetic properties of the two categories of chemical reduction nanoparticles discussed here and conventionally prepared bulk alloys merits attention in the future. Some preliminary SQUID DC-magnetisation results presented here already point to this. The fine particle character of the alloys is clearly seen in the splitting between the ZFC/FC runs. Other more subtle features, such as the low temperature kink in the ZFC curves, may be due to the interplay of various contributions such as inhomogeneous spin structures and superparamagnetic blocking. These indicate the potential scientific importance of the synthesised alloys.

Conclusions

Sodium borohydride reduction of mixed iron/zirconium sulfate solutions has been used to prepare Fe–Zr–B fine particles. The particles are black in colour and are relatively homogeneous, with stoichiometries between $Fe_{62}Zr_3B_{35}$ and $Fe_{54}Zr_{11}B_{35}$. The alloys were found to form under the following reaction conditions: a narrow pH window from 5–6, rapid stirring of the solution, addition of the borohydride solution to the mixed metal sulfates, use of degassed solvents, an Fe : Zr ratio between 4 : 1 and 20 : 1 and sodium borohydride concentrations between 0.1 and 1.2 M. If the ratio of Fe to Zr atoms in the initial mixture was set in the region of 9 : 1, the products were found to be almost entirely amorphous Fe–Zr–B alloys. For either higher or lower Fe : Zr ratios the product showed the direct synthesis of nanocrystallites of α-Fe in the fine particle amorphous Fe–Zr–B alloy. Small amounts of an Fe(II) phase and Fe(III) oxide were also detected in the products. Zr-edge EXAFS data indicated that the fine particles contained Zr in an environment that could not be assigned to Zr oxide or Zr metal but are consistent with formation of an amorphous Fe–Zr–B alloy. Samples prepared anaerobically were prone to violent oxidation and self annealing on exposure to air, generating temperatures of the order of 600 °C. Aerobically prepared particles seemed to be passivated and only underwent slow oxidation.

Acknowledgements

We thank the Leverhulme Trust for providing post doctoral support for GDF; the Spanish Ministerio de Educacion y Cultura for supporting LFB during his stay at UCL and, in partnership with the British Council, for continuing to facilitate the project *via* an Acciones Integradas grant; Neil Cohen and Marianne Odlyha of the ULIRS thermal methods group for the DSC measurements; and Mark Roberts and Graham Bushnell-Wye of the Daresbury Laboratory for their assistance with the curved image plate XRD experiments. The Mössbauer spectra in this work were recorded under the auspices of the ULIRS Mössbauer service.

References

1 A. Makino, T. Bitoh, A. Inoue and T. Masumoto, *J. Appl. Phys.*, 1997, **81**, 2736.
2 M. Kopcewicz, A. Grabias, P. Nowicki and D. L. Williamson, *J. Appl. Phys.*, 1996, **79**, 993.
3 J. M. Barandiarán, P. Gorria, I. Orue, M. L. Fdez-Gubieda, F. Plazaola, J. C. Gómez Sal, L. Fernández Barquín and L. Foures, *J. Phys.: Condens. Matter*, 1997, **9**, 5671.
4 G. Herzer, in *Handbook of Magnetic Materials Volume 10*, ed. K. H. J. Buschow, Elsevier Science, 1997, p. 415.
5 A. Slawska-Waniewska, P. Nowicki, H. K. Lachowicz, P. Gorria, J. M. Barandiarán and A. Hernando, *Phys. Rev. B*, 1994, **50**, 6465.
6 S. R. Elliott, *Physics of Amorphous Materials*, Longman, London, 1983.
7 H. H. Liebermann, in *Amorphous Metallic Alloys*, ed. F. E. Luborsky, Butterworths, London, 1983, p. 26.
8 L. Schultz and J. Eckert, in *Glassy Metals III*, ed. H.-J. Güntherodt and H. Beck, Springer Verlag, Berlin, 1994.
9 A. L. Oppergard, F. J. Darnell and H. C. Miller, *J. Appl. Phys.*, 1961, **32**, 1845.
10 H. Schlesenger, *J. Am. Chem. Soc.*, 1953, **75**, 215.
11 S. Wells, S. W. Charles, S. Morup. S. Linderoth, J. van Wonterghem, J. Larsen and M. B. Madsen, *J. Phys.: Condens. Matter*, 1989, **1**, 8199.
12 S. Linderoth and S. Morup, *J. Appl. Phys.*, 1991, **69**, 5256.
13 R. D. Ricke, *Science*, 1989, **246**, 1260.
14 A. Corrias, G. Ennas, G. Licheri, G. Marongui and G. Paschina, *Chem. Mater.*, 1990, **2**, 363.
15 J. L. Dormann, D. Fiorani and E. Tronc, *Adv. Chem. Phys.*, 1997, **97**, 283.
16 S. Morup, S. A. Sethi, S. Linderoth, C. BenderKoch and M. D. Bentzon, *J. Mater. Sci.*, 1992, **27**, 3010.
17 G. N. Glavee, K. J. Klabunde, C. M. Sorenson and G. C. Hadjipanayis, *Inorg. Chem.*, 1992, **34**, 28.
18 L. Suber, H. Romero, D. Fiorani, A. M. Testa, A. Montone, M. Vittori Antisari, J. L. Dormann, J. Maknani and N. Sparvieri, *Nanostruct. Mater.*, 1995, **6**, 949.
19 G. D. Forster, Q. A. Pankhurst and I. P. Parkin, *J. Mater. Sci. Lett.*, 1999, **18**, 39.
20 Y. Ge, G. Ying, Z. Bangwei, W. Lingling, O. Y. Yifang and L. Shuzhi, *J. Mater. Process Tech.*, 1998, **74**, 10.
21 G. D. Forster, L. Fernández Barquín, Q. A. Pankhurst and I. P. Parkin, *J. Non-Cryst. Solids*, 1999, **244**, 44.
22 M. E. Lines and M. Eibschütz, *Solid State Commun*, 1983, **45**, 435.
23 M. A. Roberts, J. L. Finney and G. Bushnell-Wye, *Mater. Sci. Forum*, 1998, **278–281**, 318.
24 EXCALIB, CLRC Daresbury Laboratory, Cheshire, UK, 1988.
25 EXBACK, CLRC Daresbury Laboratory, Cheshire, UK, 1988.
26 R. W. Grant, H. Wiedersich, A. H. Muir, Jr., U. Gonser and W. N. Delgass, *J. Chem. Phys.*, 1966, **45**, 1015.
27 B. D. Cullity, *Elements of X-Ray Diffraction*, Addison-Wesley, New York, 1960, p. 330.
28 J. Shen, Z. Li, Q. Yan and Y. Chen, *J. Phys. Chem.*, 1993, **97**, 8504.
29 K. Suzuki, A. Makino, A. Inoue and T. Masumoto, *J. Appl. Phys.*, 1991, **70**, 6232.
30 H. Hiroyoshi and K. Fukamichi, *J. Appl. Phys.*, 1982, **53**, 6923.

Paper 9/03838H